Electronic and magnetic properties of α-$FeGe_2$ films embedded in vertical spin valve devices

Dietmar Czubak [1,*] Samuel Gaucher,[1] Lars Oppermann,[1] Jens Herfort,[1] Klaus Zollner [2] Jaroslav Fabian [2]
Holger T. Grahn [1] and Manfred Ramsteiner [1,†]
[1] Paul-Drude-Institut für Festkörperelektronik, Leibniz-Instiut im Forschungsverbund Berlin e.V., Hausvogteiplatz 5-7, 10117 Berlin, Germany
[2] Institute for Theoretical Physics, University of Regensburg, 93040 Regensburg, Germany

(Received 23 June 2020; revised 2 September 2020; accepted 7 October 2020; published 26 October 2020)

We studied metastable α-$FeGe_2$, a layered tetragonal material, embedded as a spacer layer in spin valve structures with ferromagnetic Fe_3Si and Co_2FeSi electrodes. For both types of electrodes, spin valve operation is demonstrated with A metallic transport behavior of the α-$FeGe_2$ spacer layer. The spin valve signals are found to increase with both temperature and spacer thickness, which is discussed in terms of a decreasing magnetic coupling strength between the ferromagnetic bottom and top electrodes. The temperature-dependent resistances of the spin valve structures exhibit characteristic features, which are explained by ferromagnetic phase transitions between 55 and 110 K. The metallic transport characteristics as well as the low-temperature ferromagnetism are found to be consistent with the results of first-principles calculations.

DOI: 10.1103/PhysRevMaterials.4.104415

I. INTRODUCTION

Vertical spin valves are essential building blocks for spintronic applications and valuable tools for fundamental research [1,2]. After the discovery of the giant magnetoresistance effect [3], the exploration of the tunneling magnetoresistance effect heralded the next era of spin valves [4], peaking at a magnetoresistance ratio of 604% at room temperature in a device structure with MgO as spacer material [5]. Nowadays, the spacer material between the ferromagnetic electrodes becomes more and more of interest in recent research activities aiming at multifunctionalities and tunabilities of spacer materials, rather then outperforming readout efficiencies. Two-dimensional (2D) materials like transition-metal dichalcogenides [6,7] or graphene [8] have become of major interest during the last years, because of their wide range of electronic characteristics including semiconducting [9] and superconducting [10] transport behavior as well as half-metallic ferromagnetism [11].

In this paper, we introduce the layered material α-$FeGe_2$ as one of the few promising candidates regarding the search for two-dimensional spintronic materials. The successful synthesis of metastable α-$FeGe_2$ was only recently demonstrated utilizing a solid phase epitaxial process [12]. First studies on the material by electron microscopy and synchrotron x-ray diffraction revealed a layered tetragonal structure (space group $P4mm$) which can be grown quasi-two-dimensionally similar to MoS_2. Various physical properties and phenomena are proposed for α-$FeGe_2$ including magnetic phase transitions and high-T_C superconductivity [13,14]. For the counterpart α-$FeSi_2$, which so far has been much more investigated, a wide tunability of the electronic and magnetic properties has been predicted, with nonmetallic transport and ferromagnetism being observed in strain-stabilized thin films [15]. With a similar tunability of the physical properties, α-$FeGe_2$ films could be utilized both as ferromagnetic electrodes and barrier material for spintronic applications. Furthermore, the tuning of α-$FeGe_2$ might result in one of the rare 2D magnetic materials required for 2D spintronics [16–18]. However, the electronic and magnetic properties of α-$FeGe_2$ are so far basically unexplored from the experimental point of view. Since the synthesis of α-$FeGe_2$ includes the interdiffusion between amorphous Ge and an underlying Fe_3Si layer, investigations of the lateral transport and magnetometry measurements are impeded by the difficulty to avoid a remaining thin film of Fe_3Si underneath the α-$FeGe_2$ layer [19–21].

Here, we utilized vertical transport in spin valve structures to shed light on the electronic and magnetic characteristics of embedded α-$FeGe_2$ as well as test their potential for spintronic applications.

II. EXPERIMENTAL AND COMPUTATIONAL DETAILS

The investigated vertical spin valve devices are based on a trilayer structure, in which an α-$FeGe_2$ film serves as the spacer layer between a ferromagnetic bottom (FM1) and a ferromagnetic top (FM2) electrode. The trilayer structures were grown by a combination of low-temperature molecular-beam epitaxy and solid-phase epitaxy on semi-insulating GaAs(001) substrates according to an approach described previously [19,20]. The FM1 and FM2 films consist of either Fe_3Si or Co_2FeSi. The complete hybrid structures with α-$FeGe_2$ interlayers were found to be monocrystalline [12,19,20]. An overview of the sequences and thicknesses of the individual films in the investigated trilayer structures is given in Table I.

To fabricate the spin valve devices, photolithography and wet etching were used to define square pillars with a surface area of 1 μm^2 as shown in Figs. 1(a) and 1(b). The pillars

*czubak@pdi-berlin.de
†ramsteiner@pdi-berlin.de

TABLE I. Layer sequence of the trilayer structures used for the investigated spin valve devices and individual layer thicknesses.

Device	FM1	D1 (nm)	Interlayer	t (nm)	FM2	D2 (nm)
D1	Fe_3Si	36	$FeGe_2$	4	Fe_3Si	12
D2	Fe_3Si	36	$FeGe_2$	6	Fe_3Si	12
D3	Fe_3Si	36	$FeGe_2$	8	Fe_3Si	12
D4	Fe_3Si	36	$FeGe_2$	6	Co_2FeSi	12

were contacted by a Ti/Au alloy on top of insulating SiO_2, both deposited by vapor deposition. For the magnetoresistance measurements, the device resistance was measured with a fixed current of 1 mA using a three-terminal configuration as shown in Fig. 1(a). The external magnetic field was applied along a ⟨110⟩ direction of the GaAs substrate, because the detected spin valve signals showed the highest amplitude along this direction.

The electronic structure calculations were performed by density functional theory (DFT) [22] with QUANTUM ESPRESSO [23]. Self-consistent calculations were carried out with the k-point sampling of $48 \times 48 \times 36$. We performed open-shell calculations that provide the spin-polarized ground state for bulk α-$FeGe_2$. We used an energy cutoff for the charge density of 700 Ry, and the kinetic-energy cutoff for the wave functions was 80 Ry for the fully relativistic pseudopotentials employing the projector augmented-wave method [24], with the Perdew-Burke-Ernzerhof exchange-correlation functional [25]. The atomic structure of bulk α-$FeGe_2$ was taken from recent experiments [12,26]. More details about our DFT calculations are given in the Supplemental Material [27].

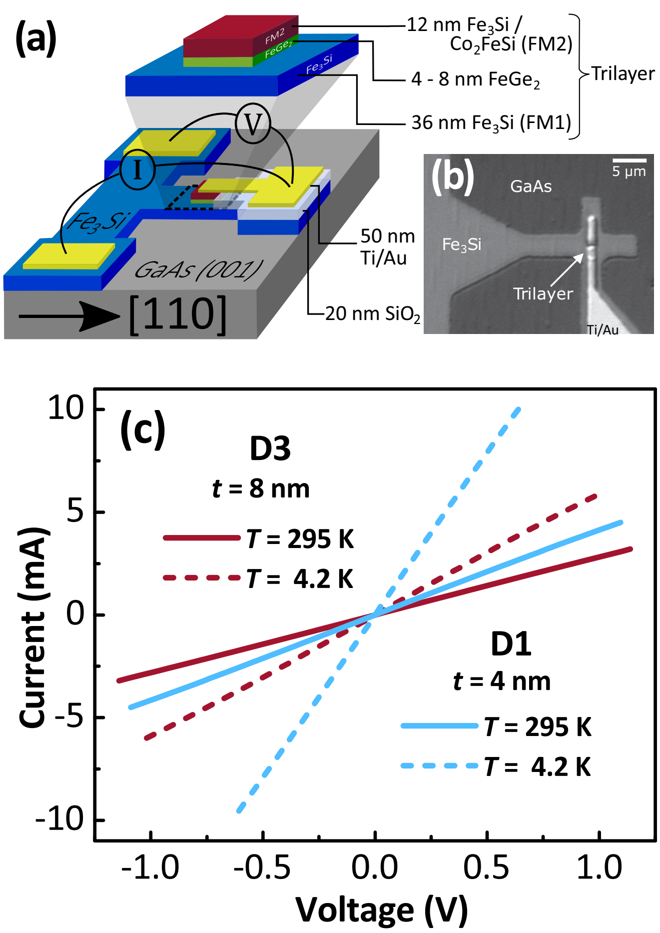

FIG. 1. (a) Schematic diagram of the device structure and the configuration of the magnetoresistance measurements for vertical transport. (b) Optical micrograph of the spin valve device. (c) Current-voltage (I-V) characteristics for devices D1 and D3 at temperatures of 295 K (solid lines) and 4.2 K (dashed lines).

III. RESULTS AND DISCUSSION

The current-voltage (I-V) characteristics for vertical transport through devices D1 and D3 are shown in Fig. 1(c). Similar results were obtained for devices D2 and D4. Nearly perfect ohmic behavior was observed at room temperature and at low temperatures with no indication of tunneling or rectification, e.g., due to the formation of a Schottky barrier at the α-$FeGe_2/FeSi_3$ interfaces. The resistance area product (RA) exhibited the expected increase for increasing the α-$FeGe_2$ spacer thickness (235 $\Omega\,\mu m^2$ for device D1 and 352 $\Omega\,\mu m^2$ for device D3) and decreased when the temperature was reduced (62 and 163 $\Omega\,\mu m^2$ for device D1 and D3, respectively). Altogether, these findings clearly prove the metallic transport behavior of the α-$FeGe_2$ film in accordance with our DFT calculations (see below). Note that, in the case of device resistances dominated by tunneling, much higher RA values and no decrease of the resistance at low temperatures would be expected [28].

The spin transport through the trilayer structures in the different devices was studied by examining the change in resistance $\Delta R(H) = R(H) - R_p$ during upward and downward sweeps of an external magnetic field (H), where R_p denotes the resistance in a large magnetic field. Figure 2(a) reveals characteristic peaks in the change of the resistance (ΔR) as signatures of successful spin valve operation for the two different FM2 materials (Co_2FeSi and Fe_3Si). The high- and low-resistance states correspond to the antiparallel and parallel magnetization configurations (FM1 vs FM2), respectively. The larger widths of the spin valve signals observed for the devices with Co_2FeSi as top electrode (device D4) are due to the higher coercive field compared to Fe_3Si [29,30]. Note that the spin valve signals are superimposed on the anisotropic magnetoresistance (AMR) caused by the lateral transport in the Fe_3Si stripes [see Fig. 1(a)] [31,32]. The occurrence of the AMR signal reflects the fact that ⟨100⟩ directions constitute the easy axes of magnetization in Fe_3Si whereas the external magnetic field is applied along a ⟨100⟩ direction. As a consequence the magnetization in the Fe_3Si stripes rotates by an angle of 45° during a sweep from large to zero magnetic field. For the determination of ΔR_{max}, the AMR contribution has been taken into account as a background signal. The larger spin valve signal detected for device D4 ($\Delta R_{max} = 0.26\ \Omega$) compared to that of device D2 ($\Delta R_{max} = 0.13\ \Omega$) is attributed to the higher spin polarization in Co_2FeSi [33,34]. The corresponding relative magnetoresistances $\Delta MR = \Delta R_{max}/R_p$ are 0.10 and 0.17% for devices D2 and D4, respectively. Note, however, that these values are influenced by the background resistance R_{FM1} originating from lateral transport in

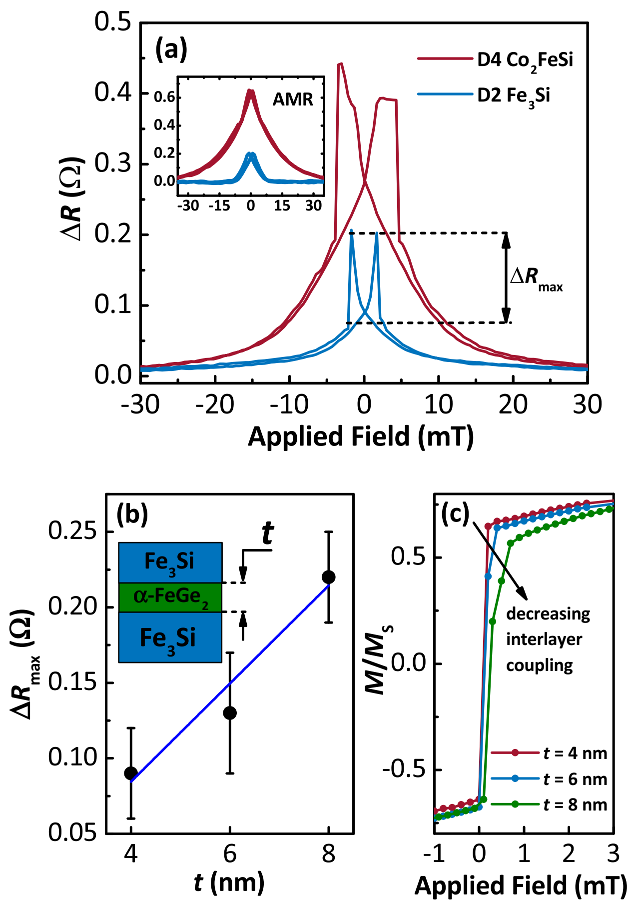

FIG. 2. (a) Change in resistance (ΔR) as a function of an external in-plane magnetic field (upward and downward sweeps) for devices D2 and D4 along the [110] direction. The inset displays the typical anisotropic magnetoresistance (AMR) signals obtained for the lateral transport in the $FeSi_3$ stripes. (b) Spin valve signal ΔR_{max} as a function of the α-$FeGe_2$ interlayer thickness t for devices D1, D2, and D3. The solid line is a guide to the eye. (c) One-way normalized SQUID magnetization curves along the [110] direction (applied field swept from negative to positive fields) for Fe_3Si/α-$FeGe_2/Fe_3Si$ samples with different spacer thicknesses. (a–c) All the presented results were measured at room temperature.

the Fe_3Si bottom layer which contributes to the magnitude of R_p.

The spin valve signal ΔR_{max} has been found to become progressively larger with increasing the thickness of the α-$FeGe_2$ interlayer as shown in Fig. 2(b). Such a monotonic increase has been previously observed for metallic spacer layers and attributed to a thickness dependent magnetic coupling between the electrodes FM1 and FM2 [35–37]. Magnetic interlayer coupling between ferromagnetic electrodes has been discussed in the literature in terms of a strong magnetostatic interaction, the density of pinholes, and Néel's orange-peel coupling [38,39]. For comparatively thin spacer layers, the interlayer coupling is expected to be relatively strong and to favor a parallel alignment of the ferromagnetic electrodes as well as a simultaneous magnetization reversal. Consequently, a complete antiparallel alignment during magnetic field sweeps is prevented which results in reduced spin valve signals. With increasing spacer thickness, the interlayer coupling strength decreases and thus also its detrimental influence on the spin valve signal, in accordance with our experimental observation. Our explanation is supported by the magnetometry measurements shown in Fig. 2(c). The magnetization reversals measured by a superconducting quantum interference device (SQUID) exhibit a clear dependence on the spacer thickness in Fe_3Si/α-$FeGe_2/Fe_3Si$ trilayer structures. The kink which develops between $M/M_s = 0$ and 0.5 with increasing spacer thickness indicates a progressing magnetic decoupling of the ferromagnetic layers [40–42]. For even larger spacer thicknesses, this kink is expected to develop into a step in the magnetization curve as a signature of fully independent magnetization reversals in the two decoupled ferromagnetic electrodes. Note that the observed coercive fields in the SQUID magnetization curves are much smaller than the range of switching fields at which the spin valve signals occur [see Fig. 2(a)]. This discrepancy is most likely due to the shape anisotropy induced during the microstructuring of the devices and additional demagnetization field effects from impurities at the contact edges [43–45]. As a consequence, the range of spacer thicknesses at which the transition from strong to weak magnetic interlayer coupling occurs is also expected to be somewhat different for large-area SQUID samples compared to microstructured spin valve devices. Although the observed spacer-thickness dependence of ΔR_{max} is consistent with metallic transport behavior, we cannot fully rule out additional spin filtering phenomena in the case of possible tunneling processes [46]. Beyond the regime of strong interlayer coupling, a decrease of the spin valve signal with increasing spacer thickness is expected according to a finite spin diffusion length in the spacer material [36,47]. Consequently, our result demonstrates that the magnetic interlayer coupling dominates over the influence of spin relaxation in the spacer for the entire range of investigated thicknesses, indicating extraordinarily strong magnetic coupling effects and a large spin-diffusion length in α-$FeGe_2$. However, the investigated spacer thicknesses are rather large compared to the previously studied cases of magnetic interlayer coupling between ferromagnetic electrodes [35–39]. Therefore, interfacial exchange coupling as an additional influence on the relative alignment of the magnetization in the ferromagnetic electrodes has to be taken into account [48]. For the occurrence of this additional mechanism, antiferromagnetic order in the α-$FeGe_2$ spacer has to be assumed, which would be in accordance with energetic considerations from DFT calculations (see Supplemental Material [27]) and the magnetic characteristic of the stable phase β-$FeGe_2$ [49]. However, further work is necessary to clarify this point.

In striking contrast to the commonly observed behavior for vertical spin valves [7,50,51], the spin valve signal of our devices vanishes with decreasing temperature as shown in Fig. 3. In fact, no characteristic spin valve signal could be detected for temperatures below 100 K. The initial decrease between room temperature and 100 K can be explained by an increasing magnetic interlayer coupling strength along the lines of the discussion above on the spacer thickness dependence. Indeed, examples of an increasing magnetic coupling strength with decreasing temperature have been reported previously [52–54]. An increase in the interlayer coupling

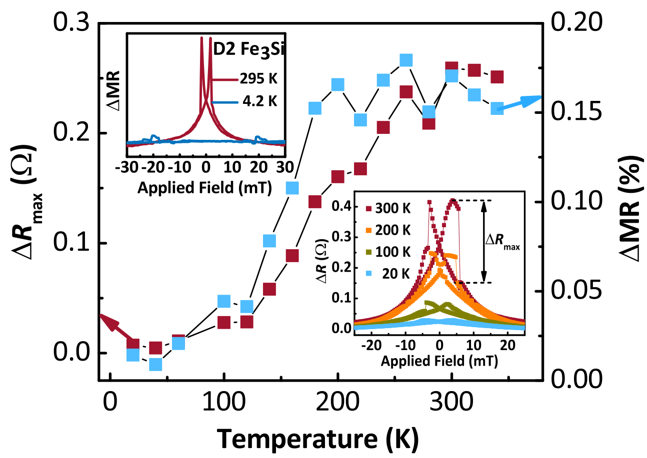

FIG. 3. Temperature dependence of the spin valve signal ΔR_{max} and the relative magnetoresistance MR for device D4. Bottom right inset: Spin valve signals of device D4 at different temperatures. Top left inset: Spin valve signals (magnetoresistances) of device D2 at 295 K (red) and 4.2 K (blue).

strength is also indicated by the slight decrease of the coercive fields at which the spin valve signals occur when lowering the temperatures (see bottom right inset of Fig. 3). The complete disappearance of the spin valve signal below 100 K is attributed to a ferromagnetic phase transition in the spacer material α-$FeGe_2$. The same quenching of the spin valve signal below 100 K has been observed for devices with Fe_3Si top electrodes (see top left inset of Fig. 3 for the case of device D2). Our DFT calculations determined the ferromagnetic phase to be the energetically most favorable one at low temperature (see discussion below). In the case of a fully ferromagnetic trilayer device structure below 100 K, a particularly strong interlayer coupling is expected leading to a simultaneous magnetization reversal in the electrodes FM1 and FM2 as well as the α-$FeGe_2$ spacer, which excludes the occurrence of a spin valve signal. Furthermore, the small spin-diffusion length commonly observed in ferromagnetic materials [55] might also contribute to the quenching of spin valve signal below the Curie temperature of α-$FeGe_2$. Note that magnetic phase transitions below room temperature were already reported for the thermodynamically stable β-$FeGe_2$ [56,57] as well as for $FeGe_2$ nanowires [58]. Furthermore, successful spin valve operation has been achieved also for the trilayer system $Fe_3Si/FeSi_2/Fe_3Si$ with a similar decrease of the device signal below 80 K [59,60].

The electronic band structure of isolated bulk α-$FeGe_2$ resulting from DFT calculations is shown in Fig. 4(a). Since the properties of thin epitaxial films are often influenced by strain, the calculations were performed for different lattice parameters: the fully relaxed structure obtained by DFT and the experimentally determined strained geometry (see Supplemental Material [27]). The resulting overall band-structure features are nearly the same for both configurations and agree reasonably well with the one reported in Ref. [12]. Additional calculations carried out for the conditions of uniaxial strain in the ⟨001⟩ and ⟨110⟩ directions up to 1% do not lead to significant changes of these band-structure features. The ab-

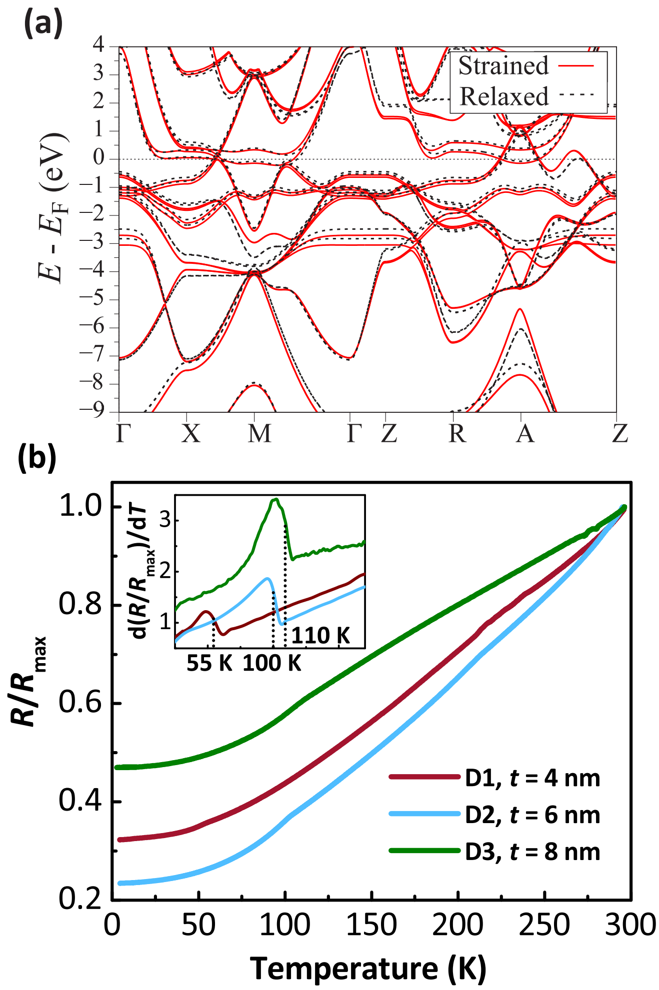

FIG. 4. (a) Calculated band structure of bulk α-$FeGe_2$ for the experimentally determined strained lattice structure according to Ref. [12] (solid line) and for the fully relaxed lattice structure determined by DFT (dashed lines). (b) Resistance normalized to its room-temperature value (R/R_{RT}) for devices D1, D2, and D3 as a function of temperature. The inset displays the corresponding temperature derivatives of the normalized resistances $[d(R/R_{RT})/(dT)]$.

sence of a band gap at the Fermi level E_F confirms our findings regarding the metallic transport characteristics (see above).

Regarding the magnetic ground state of α-$FeGe_2$, we considered three different configurations: (i) paramagnetic (PM) phase, where the atoms are considered to have no collective magnetization axis; (ii) ferromagnetic (FM) phase, in which all Fe atoms have aligned magnetic moments along the c axis; and (iii) antiferromagnetic (AFM) phase, where the ferromagnetic Fe sheets within α-$FeGe_2$ form sublattices with antiparallel order. From the total-energy analysis of these cases, we found that the FM phase is the energetically most favorable ground state. The PM phase was about 56 meV higher in energy (or about 7 meV per unit cell) compared to the FM phase, while the AFM phase was only about 2.9 meV higher in energy (or about 0.36 meV per unit cell). For the DFT-relaxed structure, the FM phase was about 35 meV (19 meV) lower in energy than the PM (AFM) phase. Again, we found that the FM phase should be the ground state. These results indicate the possibility to tune the magnetic ground state of α-$FeGe_2$ via the strain state. Note that the strain in α-$FeGe_2$ might also depend on temperature because of different thermal expansion coefficients of the film and the GaAs substrate [61,62]. This fact together with the small energy separations between the ground states of the three configurations suggest a relatively high probability for low-temperature magnetic phase transitions.

Indeed, the temperature dependence of the device resistances exhibits characteristic features which can be attributed to low-temperature ferromagnetic phase transitions. Figure 4(b) displays the resistance normalized by the resistance at room temperature R_{RT} as a function of temperature for devices D1, D2, and D3 in the magnetic virgin state with no cooling field applied. Characteristic changes in the $R/R_{RT}(T)$ curvature occur at distinct temperatures for the individual devices. The corresponding peaks in the temperature derivatives [see inset in Fig. 4(b)] can be explained by spin disorder scattering which starts to decrease below the Curie temperature T_C, where a phase change into a ferromagnetic state occurs. The accordingly determined Curie temperatures reveal thickness-dependent phase transitions occurring at 55, 100, and 110 K for spacer thicknesses of 4, 6, and 8 nm, respectively. Note that the phase transition could not be identified for device D4, most likely due to the comparatively large series resistance of the Co_2FeSi top electrode [63,64]. This result provides strong support for our explanation regarding the absence of a spin valve signal at temperatures below 100 K observed for device D4 (see Fig. 3). The determination of the ferromagnetic phase transition temperature for α-$FeGe_2$ spacer layers embedded in trilayer structures with ferromagnetic electrodes constitutes an achievement which is difficult to obtain by other means.

IV. SUMMARY AND CONCLUSIONS

The layered tetragonal material α-$FeGe_2$ embedded as a spacer layer in vertical spin valve structures exhibits metallic transport behavior. Successful spin valve operation is demonstrated for structures with ferromagnetic Fe_3Si (bottom and top) and Co_2FeSi (top) electrodes. An enhancement of the spin valve signals with increasing temperature and spacer layer thickness is attributed to a decreasing magnetic interlayer coupling between the ferromagnetic bottom and top electrodes. Characteristic features in the temperature derivatives of the device resistances are assigned to a ferromagnetic phase transition between 55 and 110 K. Both the metallic characteristics and the ferromagnetic ground state at low temperatures are confirmed by DFT calculations.

ACKNOWLEDGMENTS

K.Z. and J.F. were supported by Deutsche Forschungsgemeinschaft SFB 1277 (Grant No. 314695032). We gratefully acknowledge technical support by Walid Anders and Angela Riedel as well as the critical reading of the paper by Alberto Hernández-Mínguez.

[1] S. A. Wolf, D. D. Awschalom, R. A. Buhrman, J. M. Daughton, S. von Molnár, M. L. Roukes, A. Y. Chtchelkanova, and D. M. Treger, Science **294**, 1488 (2001).
[2] Y. P. Feng, L. Shen, M. Yang, A. Wang, M. Zeng, Q. Wu, S. Chintalapati, and C.-R. Chang, WIREs Comput. Mol. Sci. **7**, e1313 (2017).
[3] B. Dieny, V. Speriosu, B. Gurney, S. Parkin, D. Wilhoit, K. Roche, S. Metin, D. Peterson, and S. Nadimi, J. Magn. Magn. Mater. **93**, 101 (1991).
[4] J. S. Moodera, L. R. Kinder, T. M. Wong, and R. Meservey, Phys. Rev. Lett. **74**, 3273 (1995).
[5] S. Ikeda, J. Hayakawa, Y. Ashizawa, Y. Lee, K. Miura, H. Hasegawa, M. Tsunoda, F. Matsukura, and H. Ohno, Appl. Phys. Lett. **93**, 082508 (2008).
[6] W. Wang, A. Narayan, L. Tang, K. Dolui, Y. Liu, X. Yuan, Y. Jin, Y. Wu, I. Rungger, S. Sanvito, and F. Xiu, Nano Lett. **15**, 5261 (2015).
[7] M. Z. Iqbal, M. W. Iqbal, S. Siddique, M. F. Khan, and S. M. Ramay, Sci. Rep. **6**, 21038 (2016).
[8] A. K. Singh and J. Eom, ACS Appl. Mater. Interfaces **6**, 2493 (2014).
[9] T. Böker, R. Severin, A. Müller, C. Janowitz, R. Manzke, D. Voß, P. Krüger, A. Mazur, and J. Pollmann, Phys. Rev. B **64**, 235305 (2001).
[10] R. Zhang, I.-L. Tsai, J. Chapman, E. Khestanova, J. Waters, and I. V. Grigorieva, Nano Lett. **16**, 629 (2016).
[11] Y. Tong, Y. Guo, K. Mu, H. Shan, J. Dai, Y. Liu, Z. Sun, A. Zhao, X. C. Zeng, C. Wu *et al.*, Adv. Mater. **29**, 1703123 (2017).
[12] B. Jenichen, M. Hanke, S. Gaucher, A. Trampert, J. Herfort, H. Kirmse, B. Haas, E. Willinger, X. Huang, and S. C. Erwin, Phys. Rev. Mater. **2**, 051402(R) (2018).
[13] G. R. Stewart, Rev. Mod. Phys. **83**, 1589 (2011).
[14] W. Miiller, J. Tomczak, J. Simonson, G. Smith, G. Kotliar, and M. Aronson, J. Phys.: Condens. Matter **27**, 175601 (2015).
[15] G. Cao, D. J. Singh, X.-G. Zhang, G. Samolyuk, L. Qiao, C. Parish, K. Jin, Y. Zhang, H. Guo, S. Tang, W. Wang, J. Yi, C. Cantoni, W. Siemons, E. A. Payzant, M. Biegalski, T. Z. Ward, D. Mandrus, G. M. Stocks, and Z. Gai, Phys. Rev. Lett. **114**, 147202 (2015).
[16] M. Gibertini, M. Koperski, A. F. Morpurgo, and K. S. Novoselov, Nat. Nanotechnol. **14**, 408 (2019).
[17] C. Gong and X. Zhang, Science **363**, eaav4450 (2019).
[18] D. L. Cortie, G. L. Causer, K. C. Rule, H. Fritzsche, W. Kreuzpaintner, and F. Klose, Adv. Funct. Mater. **30**, 1901414 (2020).
[19] S. Gaucher, B. Jenichen, J. Kalt, U. Jahn, A. Trampert, and J. Herfort, Appl. Phys. Lett. **110**, 102103 (2017).
[20] S. Gaucher, B. Jenichen, and J. Herfort, Semicond. Sci. Technol. **33**, 104005 (2018).
[21] M. Terker, B. Jenichen, J. Herfort, and A. Trampert, Semicond. Sci. Technol. **34**, 124004 (2019).
[22] P. Hohenberg and W. Kohn, Phys. Rev. **136**, B864 (1964).

[23] P. Giannozzi, S. Baroni, N. Bonini, M. Calandra, R. Car, C. Cavazzoni, D. Ceresoli, G. L. Chiarotti, M. Cococcioni, I. Dabo, A. Dal Corso, S. de Gironcoli, S. Fabris, G. Fratesi, R. Gebauer, U. Gerstmann, C. Gougoussis, A. Kokalj, M. Lazzeri, L. Martin-Samos, N. Marzari, F. Mauri, R. Mazzarello, S. Paolini, A. Pasquarello, L. Paulatto, C. Sbraccia, S. Scandolo, G. Sclauzero, A. P. Seitsonen, A. Smogunov, P. Umari, and R. M. Wentzcovitch, J. Phys.: Condens. Matter **21**, 395502 (2009).
[24] G. Kresse and D. Joubert, Phys. Rev. B **59**, 1758 (1999).
[25] J. P. Perdew, K. Burke, and M. Ernzerhof, Phys. Rev. Lett. **77**, 3865 (1996).
[26] S. R. Bahn and K. W. Jacobsen, Comput. Sci. Eng. **4**, 56 (2002).
[27] See Supplemental Material at http://link.aps.org/supplemental/10.1103/PhysRevMaterials.4.104415 for the corresponding lattice constants.
[28] E. J. Patiño and N. G. Kelkar, Appl. Phys. Lett. **107**, 253502 (2015).
[29] J. Herfort, H.-P. Schönherr, and K. H. Ploog, Appl. Phys. Lett. **83**, 3912 (2003).
[30] M. Hashimoto, J. Herfort, H.-P. Schönherr, and K. H. Ploog, Appl. Phys. Lett. **87**, 102506 (2005).
[31] M. Bowen, K.-J. Friedland, J. Herfort, H.-P. Schönherr, and K. H. Ploog, Phys. Rev. B **71**, 172401 (2005).
[32] M. Erekhinsky, J. de la Venta, and I. K. Schuller, J. Appl. Phys. **114**, 143901 (2013).
[33] M. Ramsteiner, O. Brandt, T. Flissikowski, H. T. Grahn, M. Hashimoto, J. Herfort, and H. Kostial, Phys. Rev. B **78**, 121303(R) (2008).
[34] K. Hamaya, N. Hashimoto, S. Oki, S. Yamada, M. Miyao, and T. Kimura, Phys. Rev. B **85**, 100404(R) (2012).
[35] Th. G. S. M. Rijks, R. Coehoorn, J. T. F. Daemen, and W. J. M. de Jonge, J. Appl. Phys. **76**, 1092 (1994).
[36] J. C. S. Kools, J. Appl. Phys. **77**, 2993 (1995).
[37] J. L. Leal and M. H. Kryder, J. Appl. Phys. **79**, 2801 (1996).
[38] B. Dieny, V. S. Speriosu, S. S. P. Parkin, B. A. Gurney, D. R. Wilhoit, and D. Mauri, Phys. Rev. B **43**, 1297(R) (1991).
[39] J. C. S. Kools, Th. G. S. M. Rijks, A. E. M. De Veirman, and R. Coehoorn, IEEE Trans. Magn. **31**, 3918 (1995).
[40] C. Schanzer, V. Shah, T. Gutberlet, M. Gupta, P. Böni, and H. Braun, Phys. B: Condens. Matter **356**, 46 (2005).
[41] X. Liu, W. Liu, F. Yang, X. Lv, W. Cui, S. Guo, W. Gong, and Z. Zhang, Appl. Phys. Lett. **95**, 222505 (2009).
[42] X. Liu, W. Liu, S. Guo, W. Gong, J. Feng, and Z. Zhang, Appl. Phys. Lett. **97**, 072502 (2010).
[43] J. Fluitman, Thin Solid Films **16**, 269 (1973).
[44] M. Kryder, K. Ahn, N. Mazzeo, S. Schwarzl, and S. Kane, IEEE Trans. Magn. **16**, 99 (1980).
[45] W. Lee, Y. Xu, C. Vaz, A. Hirohata, H. Leung, C. Yao, B.-C. Choi, J. Bland, F. Rousseaux, E. Cambril *et al.*, IEEE Trans. Magn. **35**, 3883 (1999).
[46] D. C. Worledge and T. H. Geballe, J. Appl. Phys. **88**, 5277 (2000).
[47] V. S. Speriosu, J. P. Nozieres, B. A. Gurney, B. Dieny, T. C. Huang, and H. Lefakis, Phys. Rev. B **47**, 11579(R) (1993).
[48] M. Pankratova and A. Kovalev, Low Temp. Phys. **41**, 838 (2015).
[49] T. Mason, C. Adams, S. Mentink, E. Fawcett, A. Menshikov, C. Frost, J. Forsyth, T. Perring, and T. Holden, Phys. B: Condens. Matter **237**, 449 (1997).
[50] T. Kimura, T. Sato, and Y. Otani, Phys. Rev. Lett. **100**, 066602 (2008).
[51] E. Y. Tsymbal, O. N. Mryasov, and P. R. LeClair, J. Phys.: Condens. Matter **15**, R109 (2003).
[52] Y. Hu, M. Ji, J. Peng, W. Qiu, M. Pan, J. Zhao, Y. Yao, C. Han, J. Hu, L. Pan, W. Tian, D. Chen, Q. Zhang, and P. Li, J. Magn. Magn. Mater. **487**, 165317 (2019).
[53] N. Persat and A. Dinia, Phys. Rev. B **56**, 2676 (1997).
[54] Z. Zhang, L. Zhou, P. E. Wigen, and K. Ounadjela, Phys. Rev. Lett. **73**, 336 (1994).
[55] J. Bass and W. P. Pratt, Jr., J. Phys.: Condens. Matter **19**, 183201 (2007).
[56] L. M. Corliss, J. M. Hastings, W. Kunnmann, R. Thomas, J. Zhuang, R. Butera, and D. Mukamel, Phys. Rev. B **31**, 4337 (1985).
[57] V. V. Men'shenin, Phys. Solid State **61**, 421 (2019).
[58] S. Tang, I. Kravchenko, T. Z. Ward, Q. Zou, J. Yi, C. Ma, M. Chi, G. Cao, A.-P. Li, D. Mandrus, and Z. Gai, Sci. Rep. **7**, 7126 (2017).
[59] Y. Asai, K. Sakai, K. Ishibashi, K. Takeda, and T. Yoshitake, Jpn. J. Appl. Phys. Conf. Proc. **3**, 011501 (2015).
[60] K. Ishibashi, K. Kudo, K. Nakashima, Y. Asai, K. Sakai, H. Deguchi, and T. Yoshitake, Jpn. J. Appl. Phys. Conf. Proc. **5**, 011501 (2017).
[61] O. Thomas, Q. Shen, P. Schieffer, N. Tournerie, and B. Lépine, Phys. Rev. Lett. **90**, 017205 (2003).
[62] J. Mohanty, T. Hesjedal, A. Ney, Y. Takagaki, R. Koch, L. Däweritz, and K. H. Ploog, Appl. Phys. Lett. **83**, 2829 (2003).
[63] J. Herfort, H.-P. Schönherr, K.-J. Friedland, and K. Ploog, J. Vac. Sci. Technol. B **22**, 2073 (2004).
[64] M. Hashimoto, J. Herfort, H.-P. Schönherr, and K. Ploog, J. Appl. Phys. **98**, 104902 (2005).